Heterogeneous lithification across a legacy coastal slag bank: the creation of new sedimentary rock from anthropogenic material

Robin Hilderman[1]* (ID), John MacDonald[1] (ID), Sammy Griffin[1] (ID), Charlotte Slaymark[1] (ID), Joshua Einsle[1] (ID), Andrew Monaghan[2]

1   School of Geographical and Earth Sciences, University of Glasgow, United Kingdom
2   School of Chemistry, University of Glasgow, United Kingdom

*corresponding authors: Robin Hilderman (2797467h@student.gla.ac.uk)

Abstract | Lithification of artificial ground comprising by-products of legacy iron and steel workings presents a range of opportunities including atmospheric carbon dioxide (CO_2) storage. The natural environmental processes altering these waste sites can also pose challenges such as ecotoxic metal leaching, and so it is important to characterise these largely undocumented anthropogenically-derived rocks. This study documents the lithification mechanisms, as well as mineralogical and geochemical characteristics across a legacy coastal iron and steel slag deposit (in Warton, England). X-Ray diffraction (XRD) and energy dispersive X-ray spectroscopy (EDS) analysis of the slag deposit, as well as thermogravimetric analysis (TGA) of the cream-coloured material covering the deposit, shows lithification both on the top surface and the seaward side above the mean high-water mark (MHWM), which is the result of carbonate mineralisation. This process is driven by water weathering slag minerals (gehlenite, åkermanite, and pseudowollastonite), which release calcium (Ca). Ingassed and hydroxylated atmospheric CO_2 reacts with the leached Ca to form calcite that is slightly to strongly depleted in ^{13}C ($\delta^{13}C$ values: -6.4 ‰ to -22.7 ‰), following partial dissolved inorganic carbonate (DIC) equilibrium. Calcium-silicate-hydrate (CSH) precipitation was responsible for lithifying the deposit where more frequent and abundant seawater washing prevents subsequent slag mineral dissolution and carbonate precipitation. This work shows that legacy iron and steel slag deposits are prone to lithification, particularly in coastal settings. This lithification can draw down atmospheric CO_2 and has the potential to slow the release of toxic metals from CSH precipitation, enhancing the possibility for repurposing legacy industrial waste for CO_2 storage and coastal defence applications.

Lay summary | Increasing volumes of human-made waste are being generated and deposited on the ground, covering the natural land surface. While these largely undocumented deposits could help capture atmospheric CO_2, they could pose a risk to humans and the environment from possible toxic metal release. This study investigates how leftover materials from iron and steel production, solidify over time using mineralogical and geochemical analysis. A combination of processes involving water dissolved minerals from the waste and released calcium, which formed both a calcium-based mineral and a calcite mineral coating that lithified the deposit. This natural hardening by mineral coating captured atmospheric CO_2 and could be used for coastal protection.

Keywords: Lithification, Calcite, Slag, Carbonation, Legacy waste

1. Introduction

Artificial ground, resulting from humans acting as geological agents in landscape evolution (Wilkinson, 2005; Price et al., 2011; Cooper et al., 2018), is a defining characteristic of the Anthropocene. Heterogenous artificial ground, which ranges from spoil heaps from deep mining to furnace slag and waste tips (Price et al., 2011), contributed more than 316 gigatonne (Gt) of sediment in 2015, greatly surpassing the annual sediment supply by major rivers to oceans (more than 24 times) (Cooper et al., 2018). Population growth, a wider range of minerals being

exploited, and technological advancements are increasing the volume of anthropogenic sediment (Cooper et al., 2018).

As well as being significant in terms of volume, artificial ground deposits also pose a range of challenges (e.g., toxic metal contamination: Hobson et al. (2017)) but also many opportunities. Slag generated from the smelting of ore, coke, and fluxes to be casted into pig iron or used for steel making, can be reused due to its high stability and ability to neutralise acidity (Huijgen et al., 2005; Ahmedzade & Sengoz, 2009; Piatak & Ettler, 2021). The world iron and steel slag production in 2022 is estimated to be between 299 and 354 Mt, and between 172 and 263 Mt, respectively (USGS, 2023), and may increase to between 2.2 and 0.7 Gt/yr[1] by 2100 (Pullin et al., 2019). The significant quantities of historical waste produced during the Industrial Revolution in the United Kingdom (UK) could be used in circular economic practices for sustainable action (Branca et al., 2020). Possible resource recovery (Gomes et al., 2016; Habib et al., 2020) from the estimated 490 to 640 Mt of slag generated in the UK since 1875 (Renforth et al., 2011) would reduce the extraction of new raw materials (Bianco & Porisiensi, 2016). Mineral carbonation as a form of greenhouse gas removal (Sanna et al., 2014), which mimics natural weathering processes (Huijgen et al., 2005; Doucet, 2010; Gomes et al., 201), has been applied to alkaline iron and steel slags (Huijgen et al., 2005; Huijgen & Comans, 2006; Eloneva et al., 2008; Pan et al., 2012). The passive in-situ storage of atmospheric carbon dioxide (CO_2) documented in legacy slag-dominated artificial ground (Mayes et al., 2018; Pullin et al., 2019; MacDonald et al., 2023a; MacDonald et al., 2023b) aids in the removal of greenhouse gasses. Considering over 190 Mt of legacy iron and steel slag exist at current and former workings across the UK (Riley et al., 2020), and the increasing volumes of artificial ground in general (Cooper et al., 2018), it is necessary to understand the processes that alter these materials over modern times.

Given this range of potential opportunities that artificial ground may offer, it is important to understand how processes such as lithification (MacDonald et al., 2023a) affect their physical and mechanical properties. As the preservation of artificial ground is contingent on its ability to endure the transformative and erosional effects of nature and humans (Price et al., 2011), the degree of lithification of the typically loose and unconsolidated material will yield variable chemical and physical changes (MacDonald et al., 2023a). Despite this, most studies investigate the long-term fate of legacy slag deposits and focus on the carbon capture potential (Chukwuma et al., 2021), emplacement methods (Pullin et al., 2019), drainage waters geochemistry (Mayes et al., 2018), and the surrounding environment (Yi et al., 2012).

Lithification of a slag deposit by calcite precipitation, which forms through ingassed atmospheric CO_2 reacting with dissolved calcium (Ca) from the slag, has been documented at a small inland legacy slag deposit at Glengarnock, Scotland (MacDonald et al., 2023a). However, in the UK, volumetrically the majority of legacy slag is located in coastal settings (Riley et al., 2020), where more chemically complex interactions with seawater will occur.

This study documents the mechanisms driving the lithification of a coastal legacy slag-dominated artificial ground deposit through X-Ray diffraction (XRD), energy dispersive X-ray spectroscopy (EDS), thermogravimetric analysis (TGA), and stable Carbon and Oxygen isotope analysis. We present new insight into the influences that natural weathering processes and various water sources have on the lithification of artificial ground, informing repurposing strategies like atmospheric CO_2 storage (Renforth, 2019).

2. Material and methods

Slag samples were collected along a transect across the Warton slag heap in South Lancashire, England (54.129483°, -2.80018°: Figure 1), a place where iron and steel works were active from 1864 to 1929 (Riden & Owen, 1995; LCC, 2006). Historical accounts suggest the slag was piled to form sea embarkments and has continued to prevent extensive erosion at the Warton Saltmarsh (Harwood & Scott, 1999; Skelcher, 2014). All samples appear to be made of particles, or clasts, of grey slag, with a cream-coloured material between that vigorously effervesces when in contact with diluted hydrochloric acid. Samples W5, W6, W7, W8, and W9 (Figures 1B, C and S1A-E) were collected below the mean high watermark (MHWM) in the intertidal zone, and below where W13 was collected (Figure S1F). Sample W15 (Figure S1G) is from above the MHWM, in a zone washed by seawater during storms, whereas W18 (Figure S1H) was from the top surface of the deposit that experiences rainfall. Sample W20 (Figure S1I) is topographically lower and from the eastern side of the deposit, where more saline water from the inland Warton Saltmarsh interacts with rainwater-filled puddles where W23 was collected (Figure S1J).

Samples were cut using a cool-water diamond saw, pulverised with an agate mortar and pestle, and passed through a 53 micrometre (μm) sieve for TGA and XRD analysis. Cream-coloured material from between slag clasts (hypothesised to be a carbonate mineral) was sub-sampled for stable C and O isotope analysis. All analyses were conducted in labs in the College of Science and Engineering at the University of Glasgow.

Thermogravimetric analysis was conducted using an SDT Q600 (TA Instruments, USA), under Ar atmosphere at 100ml/min, with a 10° Celsius (C) per minute heating rate from 0°C to 1000°C. The weight loss at decomposition temperatures for slag components was determined using the modified Thermogravimetric analysis - derivative
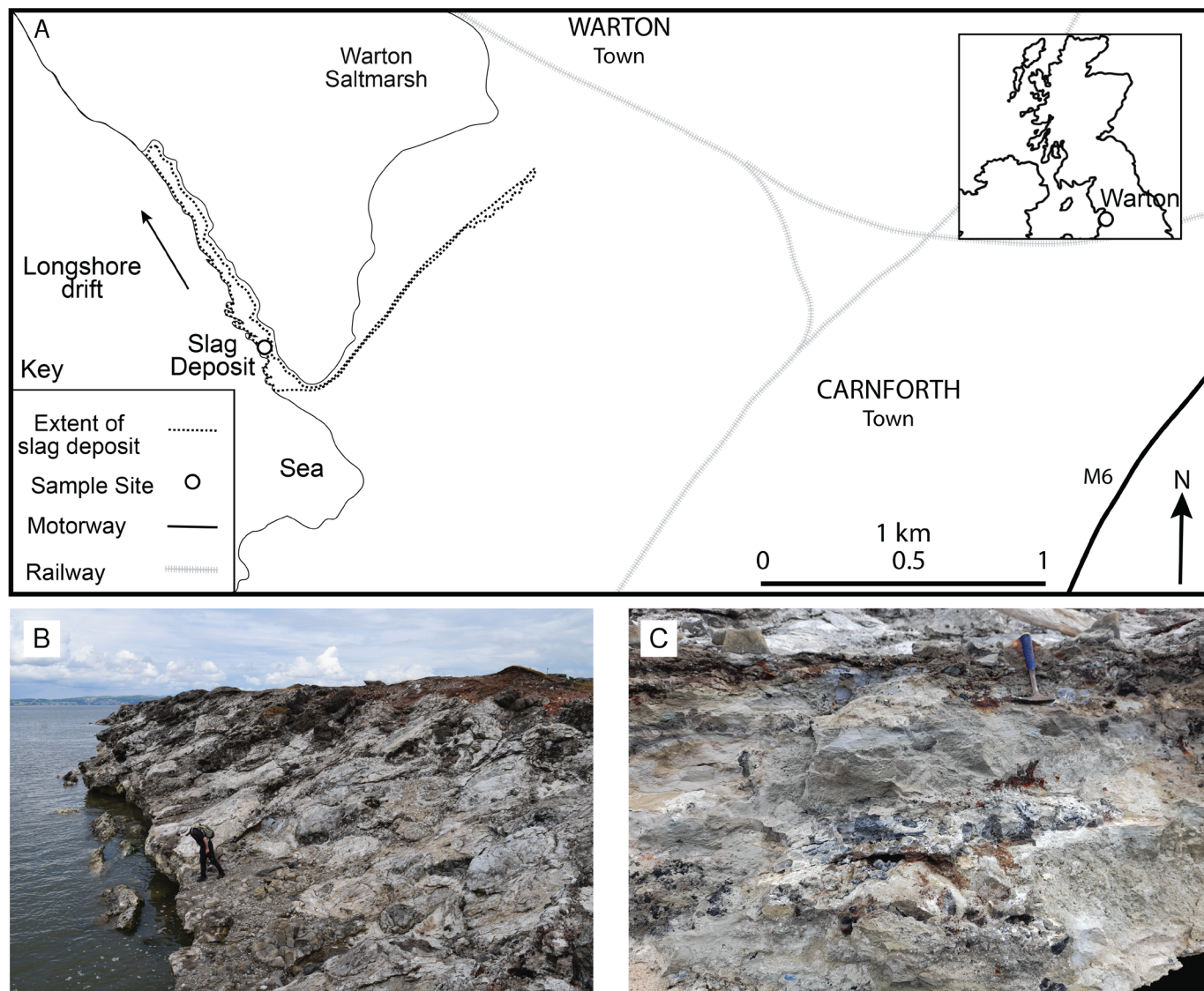
Figure 1 | (A) Location of sampling site in South Lancashire, England. (B) Field photograph showing the lithified nature of the seaward side of the approximately 10 m thick deposit; 1.82 m height person for scale. (C) Field photograph showing lithified vertical succession through the lower part of the seaward side of the deposit, where samples W5-W9 were obtained from.

TGA-DTG interpretation (Chiang & Pan, 2017) to quantify carbonate content (Table S1).

Sample mineralogy was identified by XRD on a Malvern Panalytical Empyrean, with a PIXcel3D-Medipix3 1x1 detector using Cu Kα radiation (wavelength 1.541874 (Å)). Data collection was collected in Bragg-Brentano reflection geometry 5-80° 2θ, with a step size 0.0131°. Phase identification was performed with reference to the Crystallographic Open Database (Gražulis et al., 2012).

$\delta^{13}C$ and $\delta^{18}O$ values were obtained to determine the source of CO_2 in the powdered cream-coloured material, which were acquired using an Isoprime 100 mass spectrometer. The drilled powder was acidified using phosphoric acid (≥1.90 SG) and heated for 1 hour at 60°C on an Elementar GasBench. Triplicates of the sample were run and the average reported with 1 standard deviation, except for W6 as the carbonate content was below the detection level (1 nA). The reference standards 'NBS-18' (SRM 8453) and 'IAEA-603' (IAEA) were used, and reported values were calibrated to Vienna-Pee Dee Belemnite (V-PDB).

The secondary standard IA-RO22 (Iso-Analytical Ltd.) was used to calibrate linearity for more depleted isotopic composition. Analytical uncertainty for the analysis of 0.10 and 0.18 per mille ‰ for $\delta^{13}C$ and $\delta^{18}O$, respectively, were determined from IAEA-603 (n=39) measurements during the analytical bath (Table S2A-D).

Polished thin sections, with a ~20 nm conductive carbon layer from selected samples, were imaged and mapped by SEM-EDS analysis using a Zeiss Sigma VP-FEG SEM equipped with a BSE detector, and an Oxford Instruments Ultimax 170 mm² EDS detector at the Geoanalytical Electron and Microscopy and Spectroscopy (GEMS) facility at the School of Geographical and Earth Sciences, University of Glasgow. EDS mapping was conducted with an accelerating voltage of 20 Kv, in a high vacuum using high current mode, with a working distance of 8.0 mm, and an aperture of 60 μm. EDS maps, which were acquired and processed using Oxford Instrument AZtec ® 4.3 and AZtec ® Flex software, have had the AZtec ® Trumap function applied that resolves element peak overlap and removes artefacts and background noise.

3. Results

Gehlenite ($Ca_2Al_2SiO_7$) and/or åkermanite ($Ca_2MgSi_2O_7$) (end-members of the melilite solid solution) were identified by XRD analysis (Table 1) in all but one of the ten samples, with other common slag phases such as larnite (Ca_2SiO_4) and pseudowollastonite ($CaSiO_3$) occurring in a smaller number of samples. The calcium-silicate-hydrate (CSH) minerals thaumasite ($Ca_3Si(OH)_6(CO_3)(SO_4)\cdot12H_2O$) and jouravskite ($Ca_3Mn^{4+}(SO_4)(CO_3)(OH)_6\cdot12H_2O$) occur in several samples, while all except for one sample contain carbonate minerals (dominantly calcite ($CaCO_3$), but occasionally aragonite and vaterite).

There is some correlation between mineralogy and the location of the sample along the transect from the seaward side to landward side. Notably, samples W5 and W6 from the intertidal zone contain thaumasite and jouravskite, and do not contain with calcite. Gehlenite and åkermanite are absent in W6 and fayalite ($Fe^{2+}_2SiO_4$), wüestite (FeO), and lawsonite ($CaAl_2(Si_2O_7)(OH)_2\cdot H_2O$) are associated with the elevated thaumasite and jouravskite content. The Ca-rich silicates pseudowollastonite and rankinite ($Ca_3Si_2O_7$) that occur around the MHWM (W13) are not present in samples from the top of the slag bank (W18).

Different regions of the deposit show variable textures and spatial distributions of elements within microstructures in the multi-element EDS maps from the SEM analysis (Figure 2). The slag dominantly comprises clasts that often display exsolution textures where the Si-rich portions can vary in size and concentration. The finer-grained Si-rich regions are associated with weathering slag that is Ca-poor and more porous (Figure 2A). The material cementing the slag clasts differs in size, shape, texture, and proportions of Ca and Si. The cement from below storm wave base (sample W17) is Ca-rich, varies in thickness from ~10 μm to ~ 175 μm, and forms an amorphous-shaped network that surrounds the slag clasts (Figure 2A). The cement from the intertidal zone (W1) is Si-rich and forms fine fibrous needles that both fill pores and surround Ca-rich rims on clasts edges (Figure 2B, C).

Thermogravimetric analysis of the slag samples recorded weight loss spanning 628°C to 759°C, with carbonate content reaching 16.2 weight (wt) % on the top of the bank (W18), which decreased towards the seaward side to 0.6 wt% in sample W5 (Figure 3). Weight loss exceeding 105°C associated with the expulsion of surface water up to 200°C, and the dehydration of crystalline water from weight loss between 400°C to 500°C, confirms the presence of the CSH in samples W5 and W6. Carbon and oxygen isotopic analysis of the powdered cream-coloured material from between, and around, the slag clasts gave $\delta^{13}C$ values between -6.4 ‰ and -22.7 ‰, and $\delta^{18}O$ between -4.2 ‰ and -11.3 ‰ (Figure 3 and Table 2). There is a correlation between samples with lower $\delta^{13}C$ values (-22.6 ‰: W7) in closer proximity to the sea, whereas samples from the top of the slag bank (farther from the sea) were less depleted in ^{13}C (-6.4 ‰: W18). The sample from within a puddle on the saltmarsh side of the deposit (W23) is similarly depleted to that of those exposed to seawater during storms (W15).

4. Discussion

Visual inspection during fieldwork indicates the seaward side of the deposit, comprising a sloping bank experiencing sea washing, has more cream-coloured material covering the slag than on the top of the heap. A similar study found lithifying rock-like masses of slag associated with the Glengarnock Steelworks in North Ayrshire in Scotland, which were shown to be dominated by calcite (MacDonald et al., 2023a). Calcium from the edges of the slag clasts, which sourced the calcite cement, was leached by water (Mayes et al., 2018; MacDonald et al., 2023a) from the Kilbirnie Loch (a freshwater lake) as

Sample	W5	W6	W7	W8	W9	W13	W15	W18	W20	W23
Gehlenite	*	-	*	*	*	*	*	*	*	*
Åkermanite	*	-	*	*	*	-	*	*	-	*
Calcite	-	-	*	*	*	*	*	*	*	*
Aragonite	*	-	-	-	*	-	-	-	-	-
Vaterite	-	-	*	*	-	-	-	-	*	-
Quartz	*	-	-	-	-	*	-	*	-	-
SiO2	-	*	-	-	-	-	-	-	-	-
Rankinite	-	-	-	-	-	*	-	-	-	*
Larnite	-	-	*	-	-	-	-	-	-	-
Fayalite	-	*	-	-	-	-	-	-	-	-
Wüestite	-	*	-	-	-	-	-	-	-	-
Lawsonite	-	*	-	-	-	-	-	-	-	-
Jouravskite	*	*	*	*	-	-	*	-	-	-
Thaumasite	*	*	-	-	-	-	*	-	-	-
Ettringite	-	-	-	-	-	-	-	-	*	-
Pseudo-wollastonite	-	-	-	*	*	*	-	-	*	-

Table 1 | Mineral phases identified by XRD of slag from South Lancashire, England. Symbols: * = detected; - = not detected.
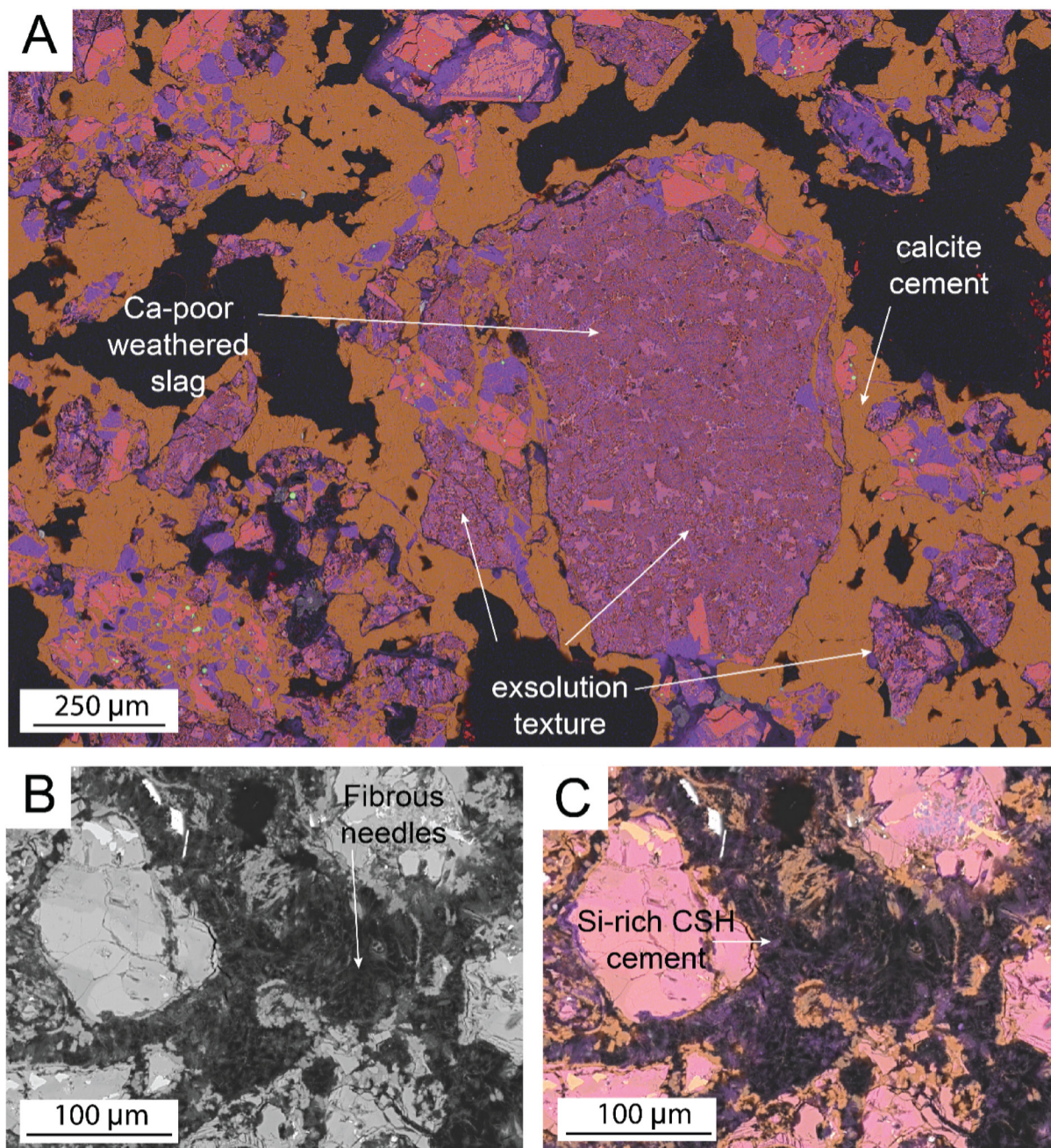
Figure 2 | SEM analysis of microstructures. (A) EDS map (orange = Ca; purple = Si; blue = Mg; red = Al; green = Fe) showing calcite cement lithifying slag clasts. Weathered slag is Ca-poor, where there is a Si-rich exsolution texture. (B) BSE image showing fibrous needle structures between slag clasts. (C) EDS map of the same area as B, showing the Si-rich CSH cement lithifying slag clasts.

in Equation 1 (1: Mayes et al., 2018; Pullin et al., 2019), where the slag forms approximately a quarter of the lake shoreline.

(1) $Ca_2SiO_4 + 4H_2O \rightleftharpoons 2Ca^{2+} + 4H4SiO4 + 4OH^-$

As the lake water drove calcite precipitation, the fluctuating lake level allowed for leached Ca to react with temporarily-isolated highly alkaline water that was pooling on the rough surface of the slag heap, promoting the ingassing and hydroxylation of atmospheric CO_2. The low negative $\delta^{13}C$ value that was recorded at Glengarnock (-20.05±0.23 ‰) supports the interpretation in this study that the calcite cement comprises atmospheric CO_2, and that there was minor dissolved inorganic carbon (DIC) equilibration in the pooled water prior to calcite precipitation (MacDonald et

al., 2023a). While the stockpiled slag from Glengarnock is in an inland lake, most legacy iron and steel slags in the UK were deposited in coastal settings (Riley et al., 2020) such as Warton, where the mechanisms and drivers of lithification may be more complex.

4.1. Mechanisms of lithification

4.1.1. Calcite cement precipitation

The cream-coloured material covering the slag heap and the cementing of clasts is the result of lithification mechanisms that are driven by Ca leaching from the presence of water (MacDonald et al., 2023a). While Ca leaching from the edge of slag clasts provides the mechanism for sourcing Ca for the calcite cement (sensu

Sample	δ¹³C (‰) VPDB	SD	δ¹⁸O (‰) VPDB	SD	Mineralogy
W5	-8.0	0.6	-4.2	0.6	Åkermanite, aragonite, gehlenite, jouravskite, thaumasite, quartz
W6	-	-	-	-	Fayalite, jouravskite, lawsonite, thaumasite, quartz, wüestite
W7	-22.7	0.1	-9.8	0.4	Åkermanite, calcite, gehlenite, jouravskite, larnite, vaterite
W8	-21.8	0.5	-7.7	0.2	Åkermanite, calcite, gehlenite, jouravskite, larnite, pseudowollastonite, vaterite
W9	-18.4	0.4	-10.7	0.1	Åkermanite, aragonite, calcite, gehlenite, pseudowollastonite
W13	-14.1	0.6	-7.1	0.2	Calcite, gehlenite, pseudowollastonite, rankinite, quartz
W15	-11.4	0.7	-11.3	0.5	Åkermanite, aragonite, calcite, gehlenite, jouravskite, thaumasite
W18	-6.4	0.2	-7.6	0.1	Åkermanite, calcite, gehlenite, quartz
W20	-14.1	1.8	-9.8	0.2	Calcite, ettringite, gehlenite, pseudowollastonite, vaterite
W23	-11.0	0.2	-8.0	1.0	Åkermanite, calcite, gehlenite, rankinite

Table 2 | δ¹³C and δ¹⁸O values of the cream-coloured material and the mineralogy of the associated slag clast.
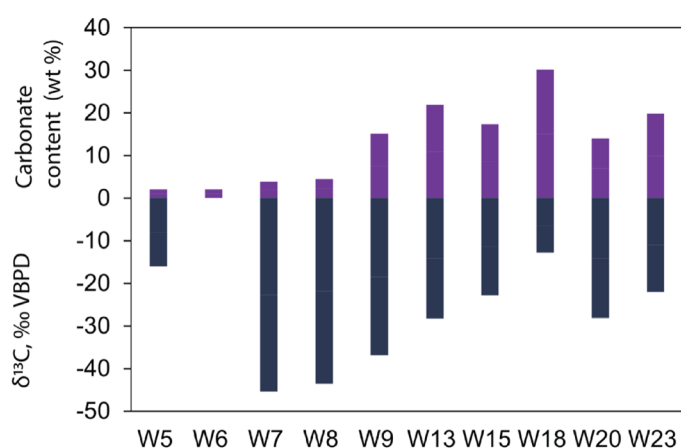
Figure 3 | Carbonate content of the slag samples, as well as δ¹³C values of the cream- coloured material from TGA and stable isotope analysis, respectively. No δ¹³C data for W6.
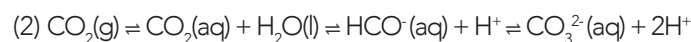
MacDonald et al., 2023a) across the three distinct regions of the slag bank (Figure 4), it is impacted by conditions that vary across the width of the deposit. The source of Ca is dependent on the solubility of the minerals comprising the slag (Huijgen et al., 2005), thus affecting lithification mechanisms. Samples from the top of the slag bank (Figure 4A) are dominated by melilite group end-members gehlenite and åkermanite, with the cement material recording 15.08 wt% calcite. On the seaward side (Figure 4B, C), additional Ca-rich phases (e.g., larnite, lawsonite, pseudowollastonite, and rankinite) were detected (Table 1), and the calcite content in the cement reached 10.9 wt% (W13). Notably, as calcite content in the cement decreases westerly along the transect with increasing proximity to the sea, the δ¹³C values become more depleted (except for W5; Figures 4 and 5). Together, these results suggest that the influence of environmental parameters on calcite precipitation are larger drivers than the mineralogy for the lithification of slag deposits.

4.1.1.1. pH

The carbonation of the slag surface is controlled by the diffusion of Ca through the solid matrix to the surface, implying mineral solubility affects the secondary precipitation of carbonate cement (Huijgen et al., 2005).

Due to the crystal structure, the dissolution of gehlenite and åkermanite is generally slower at higher pH values (gehlenite at pH 7 and pH 10; åkermanite at pH 7; Engström et al., 2013). Combined with the larger driving force for Ca dissolution compared to that of Mg at neutral to alkaline pH (Engström et al., 2013), rainwater can drive Ca leaching and increase the alkalinity (Figure 4A and Equation 1). Similar to at Glengarnock, pooling rainwater caught on the rough surface of the slag heap (MacDonald et al., 2023a) refreshed the water and slowed the increase in pH. This would explain the higher calcite content (15.08 wt%) observed from the top of the slag bank. However, calcite precipitating from a stream draining a slag heap at Consett, U.K. with a pH of >11, which was attributed to the ingassing and hydroxylating of atmospheric CO_2, demonstrates that sufficient Ca can be released from the slag for carbonate mineralisation (Mayes et al., 2018).

As demonstrated in Equation 1, the leached Ca^{2+} increases water alkalinity, promoting the ingassing of atmospheric CO_2 into solution where it is hydroxylated and precipitated as solid calcium carbonate (Equations 2 and 3) (MacDonald et al., 2023b; Mayes et al., 2018). This calcium carbonate cement lithifies the slag clasts.

(2) $CO_2(g) \rightleftharpoons CO_2(aq) + H_2O(l) \rightleftharpoons HCO^-(aq) + H^+ \rightleftharpoons CO_3^{2-}(aq) + 2H^+$

(3) $2Ca^{2+} + 2HCO^-(aq) \rightleftharpoons CaCO_3(s) + H_2O(l) + CO_2(aq)$

4.1.1.2. Seawater

Frequent and abundant seawater that acted to introduce more Mg^{2+} on the seaside of the deposit (Figure 4A, B), especially around the MHWM, created a buffer condition (Equation 4: Miki et al., 2004) to the rising pH from slag dissolution (Equation 1).

(4) $CaO(s) + H_2O + Mg_2(aq)+ \rightleftharpoons Ca^{2+}(in\ seawater) + Mg(OH)_2(s)$
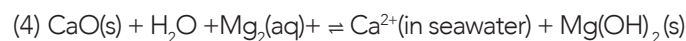
These more neutral conditions would facilitate faster Ca dissolution from gehlenite and åkermanite (Engstrom et al., 2013), enabling more carbonate precipitation. The EDS map (Figure 2A) indicates that Ca leaching from the edge of slag clasts is precipitating to form the calcite cement.
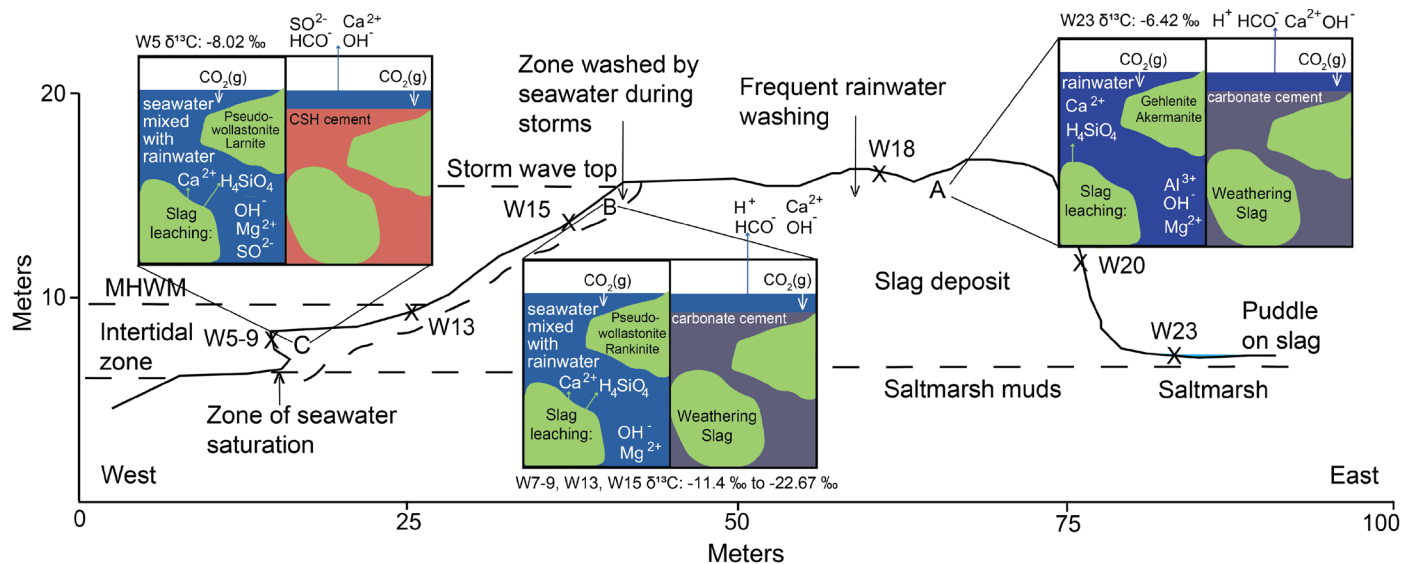
Figure 4 | Conceptual model of the mechanism lithifying slag-dominated artificial ground. (A) Rainwater facilitating melilite dissolution, which drives carbonation precipitation. (B) Rain and seawater facilitating more Ca-rich phase (pseudowollastonite and rankinite) dissolution by buffering the rising pH. (C) Seawater driving secondary CSH precipitation where erosion is undercutting the deposit.

Furthermore, when more available Ca can continuously dissolve and react with ingassed CO_2, more atmospheric CO_2 can be captured and stored in the carbonate cement (Equations 2 and 3), as evident in the low $\delta^{13}C$ values (-11.4 ‰ to -22.7 ‰: W7, W8, W9) from the seaward side of the slag bank (Figure 4B).

4.1.1.3. Atmospheric CO_2 input

The range of $\delta^{13}C$ values from the two regions of the slag bank (Figure 4A, B), where calcite cement is lithifying the deposit, indicates multiple processes affect the isotope composition. Given there is minimal vegetation on the slag deposit, and that the calcite precipitation is in-situ, there is little to no scope for biogenic carbon input; therefore, the carbon was most likely atmospheric CO_2 and was ingassed and hydroxylated prior to calcite precipitation. The low $\delta^{13}C$ values of -18.5‰ and -14.1‰ (W9 and W20, respectively) fall within the range of partially-dissolved inorganic carbon (DIC) equilibrium (Figure 5) from calcites in a hyperalkaline setting of springs in the Seminal Ophiolite in Oman (Falk et al., 2016), which is similar to the carbonated slag with hydroxylated atmospheric CO_2 from Glengarnock (-20.05 ± 0.23 ‰: MacDonald et al., 2023a). Hydroxylation and instant calcite precipitation would yield $\delta^{13}C$ values between -25‰ to -27.5‰ (Dietzel et al., 1992; Renforth et al., 2009; Falk et al., 2016) suggesting the DIC remained in solution long enough for gradual DIC equilibrium to proceed, resulting in the more intermediate isotopic composition (Falk et al., 2016). The slightly higher, less ^{13}C depleted $\delta^{13}C$ values, ranging from -14.1 ‰ to -6.4 ‰. could reflect calcite with DIC $\delta^{13}C$ values that were closer to equilibrium values following precipitation, which were then recrystallised with hydroxylated atmospheric CO_2 (Falk et al., 2016). Therefore, the $\delta^{13}C$ values from the calcite cement lithifying the slag at Warton are interpreted to reflect the ingassing and hydroxylation of atmospheric CO_2 where partial DIC equilibrium occurred prior to initial

calcite cement precipitation, followed by subsequent calcite recrystallisation.

4.1.2. Calcium-silicate-hydrate cement precipitation

Similar cream-coloured material found covering the slag heap in the intertidal zone (Figure S1A) resembling the secondary calcite cement is interpreted to consist dominantly of calcium-silicate-hydrate (CSH). The samples with the CSH phases jouravskite and thaumasite (W5 and W6) recorded more weight loss over 50°C to 200°C during TGA analysis, which is interpreted to correspond to CSH decomposition (Pane & Hansen, 2005; Haha et al., 2011; Jiang et al., 2018). This is compared to that from calcium carbonate over 600°C to 750°C (Chiang & Pan, 2017). The sulphur possibly was sourced from the original ore rock, inclusions in melilites commonly found in blast furnace slag (Scott et al., 1986; Pullin et al., 2019), or from dissolved species in seawater (Gregor et al., 1988). In a similar way, the same drivers that impact the calcite cement described above likely affect the CSH cement. The associated phases pseudowollastonite and larnite possibly contribute Ca leached by seawater. However, only slightly depleted $\delta^{13}C$ values (-8.02 ‰) from the cement suggest the CSH phases affect subsequent calcite precipitation involving atmospheric CO_2.

4.1.2.1. Surface reaction

The Ca dissolved from the slag minerals, which is from and/or diffuses to the slag surface (Huijgen et al., 2005), required a sufficient surface area to be able to precipitate (Ragipani et al., 2019). In this study, we found CSH preferentially precipitates over calcite in the intertidal zone (Figure 4C). The BSE and EDS map shows the Si-rich fibrous needles surrounding slag clasts, with Ca-rich rims that cement the clasts together (Figure 2B, C). The CSH acts as a Ca sink for ions that would have been used
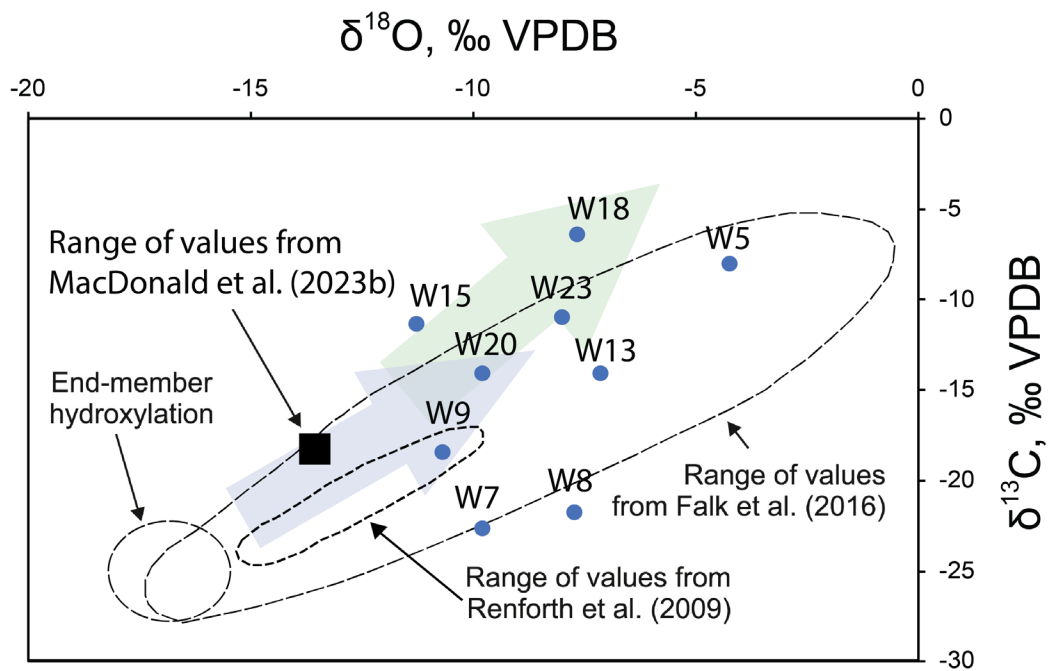
Figure 5 | $\delta^{13}C$ and $\delta^{18}O$ values from this study (blue circles) and analogous studies (Renforth et al., 2009; Falk et al., 2016); partial DIC equilibrium (blue arrow) and recrystallisation (green arrow) trends, as well as hydroxylation fields from (Falk et al., 2016). Modified from (MacDonald et al., 2023b).

to form carbonates (Béarat et al., 2006) and reduces the permeability of the slag (Pullin et al., 2019). A hydration front between secondary CSH surrounding a Ca-, Si-, and S-depleted inner alteration layer, where the most reactive phases (i.e., larnite) were absent, indicates water diffusion is limited in carbonated slag (Pullin et al., 2019). Without sufficient water to drive the leaching of Ca (MacDonald et al., 2023a) following CSH formation (that is reducing exposed slag) subsequent calcite cement precipitation is unlikely. Similar weathering documented in a basic oxygen furnace slag, with larnite dissolution and CSH precipitation (Hobson et al., 2017), supports secondary CSH precipitation as the mechanism lithifying the heap in the intertidal zone.

4.1.2.2. Atmospheric CO_2 input

The $\delta^{13}C$ values from calcite in samples with CSH fall outside the range of values from samples located on the top of the deposit, except for that from W18. Calcite is a minor component in these samples, with CSH from the intertidal zone. Recrystallisation of the CSH comprising ingassed and hydroxylated atmospheric CO_2 that underwent partial DIC equilibrium could explain the deviation of $\delta^{13}C$ values from the hydroxylation end-member (-25‰; Dietzel et al., 1992).

4.2. Implications

The lithification mechanisms documented in this study are driven by the two compositionally distinct regions of the slag bank. With increasing volumes of artificial ground produced annually (Cooper et al., 2018), understanding how these deposits interact with the environment following deposition will inform repurposing

capabilities and possible remediation measures. The composition of artificial ground will continue to change alongside the technological advancements that now allow modern extraction techniques to exploit lower quality resources (Cooper et al., 2018). Historic accounts claiming the slag bank has prevented coastal erosion of the Warton Saltmarsh support the use of slag for 'hard' protection and coastal defence once lithified (Pranzini & Williams, 2013; Riley et al., 2020). Furthermore, slag replacement in Portland Cement has been found to reduce the degradation from sulphate attack by reducing the cement permeability (McGrath & Hooton, 1997) as a result of the dense microstructures of slag (Brown et al., 2003). Cement with a higher slag content was found to be more effective at reducing sulphate attack due to shallow ettringite formation (Brown et al., 2003). While the CSH documented in this study has been shown to improve the durability of steel slag building materials (Lizarazo-Marriaga et al., 2011; Zhang et al., 2011), the physical integrity of cement is often compromised from ettringite and thaumasite formation (Mehta, 1983; Shi et al., 2012). The expansion and cracking from secondary ettringite (Mehta, 1983; Tian & Cohen, 2000), cement degradation in marine environments attributed to thaumasite formation (Irassar et al., 2003), and decreased strength in concrete with ettringite and thaumasite (Tian & Cohen, 2000; Shi et al., 2012) highlight the importance of understanding how lithified slag of varying compositions evolves in the presence of seawater.

The mechanisms responsible for the lithification of slag-dominated artificial ground present the opportunity to remove atmospheric CO_2. Using the reported density range minimum of BF (1150 to 1440kg/m³), maximum of BOF (1600 to 1760kg/m³) slag (sensu Lee, 1974), and the

average percentage of carbonate of the total sample mass (7.95 %), the estimated carbon sequestration potential is 38,694 to 59,218 t of CO_2. Even with less carbonate precipitation where the slag is more frequently washed by seawater, more atmospheric CO_2 is drawn down and mineralised. However, as a result of the armouring effect from CSH precipitation and the resulting reduction in surface reaction (Ragipani et al., 2019) that limits slag mineral dissolution and available Ca, additional sources of Ca and agitation to restore the surface reaction are necessary for subsequent CO_2 mineralisation. Calculation of the CO_2 capture potential of lithified slag-dominated artificial ground must consider how secondary precipitates affect the total extent and rate of carbonation (Hobson et al., 2017). Additionally, experiments to determine the impact that mineralogy has on atmospheric CO_2 capture could further elucidate the processes responsible for the variable $\delta^{13}C$ values that deviate from the hydroxylation end member.

Nevertheless, the cream-coloured material covering the slag bank identified as secondary CSH may mitigate one of the challenges posed by artificial ground. The dissolution of slag minerals comprising potentially toxic elements such as V and Cr (Mayes et al., 2018) is limited by the armouring effect from CSH formation. Even though the tetrahedral Si site of dicalcium silicate can accommodate V(V), the presence of V(V) in secondary CSH suggests the released vanadate was reincorporated (Hobson et al., 2017). Furthermore, the long-term release of Cr from steel slag, and other alkaline wastes in similar open systems controlled by the solubility of secondary CSH release, tends to be in stable forms. The incorporation of Cr(III) into CSH during leaching experiments has been shown to prevent oxidation in the solid slag matrix (De Windt et al., 2011). Therefore, the lithification of slag-dominated artificial ground by secondary CSH precipitation may prevent the release of toxic metals at ambient conditions.

5. Conclusions

This study identifies the mechanisms that acted to lithify a coastal legacy iron and steel slag deposit in South Lancashire, England. Compositionally diverse (identified by XRD) slag samples spanning the width of the deposit are lithified by cream-coloured material with variable calcite content (confirmed by TGA), and contain a range of $\delta^{13}C$ values.

On the top of the deposit, rainfall dissolved gehlenite and åkermanite, promoting Ca leaching and atmospheric CO_2 mineralised into the calcite cement that lithifies this region. Comparatively, where there are more Ca-rich phases that are washed by seawater on the seaward side of the deposit above the MHWM, there is less calcite, and this calcite records lower $\delta^{13}C$ values. Secondary CSH that covers and lithifies the deposit below the MLWM, inhibits further mineral dissolution and carbonation, potentially limiting the release of toxic metals.

The identified mineralogical and external environmental parameters influencing slag lithification suggest the opportunities for atmospheric CO_2 capture and reuse for 'hard protection' and coastal defence applications. The repurposing and management of slag-dominated artificial ground could be optimised to facilitate in-situ atmospheric CO_2 capture by mineralisation.

Authors contribution

Robin Hilderman: Investigation, Formal analysis, Data curation, Writing - original draft, Visualization. John M. MacDonald: Conceptualization, Methodology, Investigation, Validation, Writing - review & editing, Funding acquisition. Sammy Griffin: Data collection; Joshua Einsle: Writing - review & editing; Charlotte Slaymark: Data collection. Andy Monaghan: Data collection.

Data availability

The authors confirm that the data supporting the findings of this study are available within the article and in the supplementary material.

Conflict of interest

The authors declare that they have no known competing financial interests or personal relationships that influence the work reported in this paper.

References

Ahmedzade, P., & Sengoz, B. (2009). Evaluation of steel slag coarse aggregate in hot mix asphalt concrete. Journal of Hazardous Materials, 165(1), 300–305. https://doi.org/10.1016/j.jhazmat.2008.09.105

Béarat, H., McKelvy, M. J., Chizmeshya, A. V. G., Gormley, D., Nunez, R., Carpenter, R. W., Squires, K., & Wolf, G. H. (2006). Carbon Sequestration via Aqueous Olivine Mineral Carbonation: Role of Passivating Layer Formation. Environmental Science & Technology, 40(15), 4802–4808. https://doi.org/10.1021/es0523340

Bianco, L., & Porisiensi, S. (2016). Economia circolare e Sostenibilità. 10.

Branca, T. A., Colla, V., Algermissen, D., Granbom, H., Martini, U., Morillon, A., Pietruck, R., & Rosendahl, S. (2020). Reuse and Recycling of By-Products in the Steel Sector: Recent Achievements Paving the Way to Circular Economy and Industrial Symbiosis in Europe. Metals, 10(3), Article 3. https://doi.org/10.3390/met10030345

Brown, P. W., Hooton, R. D., & Clark, B. A. (2003). The co-existence of thaumasite and ettringite in concrete exposed to magnesium sulfate at room temperature and the influence of blast-furnace slag substitution on sulfate resistance. Cement and Concrete Composites, 25(8), 939–945. https://doi.org/10.1016/S0958-9465(03)00152-5

Chiang, P.-C., & Pan, S.-Y. (2017). Carbon dioxide mineralization and utilization. Springer.

Chukwuma, J. S., Pullin, H., & Renforth, P. (2021). Assessing the carbon capture capacity of South Wales' legacy iron and steel slag. Minerals Engineering, 173, 107232. https://doi.org/10.1016/j.mineng.2021.107232

Cooper, A. H., Brown, T. J., Price, S. J., Ford, J. R., & Waters, C. N. (2018). Humans are the most significant global geomorphological driving force of the 21st century. The Anthropocene Review, 5(3), 222–229. https://doi.org/10.1177/2053019618800234

LCC. (2006). Lancashire Historic Town Survey Programme: Preston with Walton-le-Dale and Penwortham, Historic Town Assessment Report.

De Windt, L., Chaurand, P., & Rose, J. (2011). Kinetics of steel slag leaching: Batch tests and modeling. Waste Management, 31(2), 225–235. https://doi.org/10.1016/j.wasman.2010.05.018

Dietzel, M., Usdowski, E., & Hoefs, J. (1992). Chemical and 13C/12C- and 18O/16O-isotope evolution of alkaline drainage waters and the precipitation of calcite. Applied Geochemistry, 7(2), 177–184. https://doi.org/10.1016/0883-2927(92)90035-2

Doucet, F. J. (2010). Effective CO2-specific sequestration capacity of steel slags and variability in their leaching behaviour in view of industrial mineral carbonation. Minerals Engineering, 23(3), 262–269. https://doi.org/10.1016/j.mineng.2009.09.006

Eloneva, S., Teir, S., Salminen, J., Fogelholm, C.-J., & Zevenhoven, R. (2008). Fixation of CO2 by carbonating calcium derived from blast furnace slag. Energy, 33(9), 1461–1467.

Engström, F., Adolfsson, D., Samuelsson, C., Sandström, Å., & Björkman, B. (2013). A study of the solubility of pure slag minerals. Minerals Engineering, 41, 46–52. https://doi.org/10.1016/j.mineng.2012.10.004

Falk, E. S., Guo, W., Paukert, A. N., Matter, J. M., Mervine, E. M., & Kelemen, P. B. (2016). Controls on the stable isotope compositions of travertine from hyperalkaline springs in Oman: Insights from clumped isotope measurements. Geochimica et Cosmochimica Acta, 192, 1–28. https://doi.org/10.1016/j.gca.2016.06.026

Gomes, H. I., Mayes, W. M., Rogerson, M., Stewart, D. I., & Burke, I. T. (2016). Alkaline residues and the environment: A review of impacts, management practices and opportunities. Journal of Cleaner Production, 112, 3571–3582. https://doi.org/10.1016/j.jclepro.2015.09.111

Gražulis, S., Daškevič, A., Merkys, A., Chateigner, D., Lutterotti, L., Quirós, M., Serebryanaya, N. R., Moeck, P., Downs, R. T., & Le Bail, A. (2012). Crystallography Open Database (COD): An open-access collection of crystal structures and platform for world-wide collaboration. Nucleic Acids Research, 40(D1), D420–D427. https://doi.org/10.1093/nar/gkr900

Gregor, C. B., Garrels, R. M., Mackenzie, F. T., & Maynard, J. B. (1988). Chemical Cycles in the Evolution of the Earth. Wiley New York.

Habib, A., Bhatti, H. N., & Iqbal, M. (2020). Metallurgical Processing Strategies for Metals Recovery from Industrial Slags. Zeitschrift Für Physikalische Chemie, 234(2), 201–231. https://doi.org/10.1515/zpch-2019-0001

Haha, M. B., Lothenbach, B., Le Saout, G., & Winnefeld, F. (2011). Influence of slag chemistry on the hydration of alkali-activated blast-furnace slag — Part I: Effect of MgO. Cement and Concrete Research, 41(9), 955–963. https://doi.org/10.1016/j.cemconres.2011.05.002

Harwood, T. R., & Scott, R. (1999). A report on Spartina anglica control Grange-over-Sands 1998-1999 for South Lakeland District Council.

Hobson, A. J., Stewart, D. I., Bray, A. W., Mortimer, R. J. G., Mayes, W. M., Rogerson, M., & Burke, I. T. (2017). Mechanism of Vanadium Leaching during Surface Weathering of Basic Oxygen Furnace Steel Slag Blocks: A Microfocus X-ray Absorption Spectroscopy and Electron Microscopy Study. Environmental Science & Technology, 51(14), 7823–7830. https://doi.org/10.1021/acs.est.7b00874

Huijgen, W. J. J., & Comans, R. N. J. (2006). Carbonation of Steel Slag for CO 2 Sequestration: Leaching of Products and Reaction Mechanisms. Environmental Science & Technology, 40(8), 2790–2796. https://doi.org/10.1021/es052534b

Huijgen, W. J. J., Witkamp, G.-J., & Comans, R. N. J. (2005). Mineral CO 2 Sequestration by Steel Slag Carbonation. Environmental Science & Technology, 39(24), 9676–9682. https://doi.org/10.1021/es050795f

Irassar, E. F., Bonavetti, V. L., & González, M. (2003). Microstructural study of sulfate attack on ordinary and limestone Portland cements at ambient temperature. Cement and Concrete Research, 33(1), 31–41. https://doi.org/10.1016/S0008-8846(02)00914-6

Jiang, N.-J., Du, Y.-J., & Liu, K. (2018). Durability of lightweight alkali-activated ground granulated blast furnace slag (GGBS) stabilized clayey soils subjected to sulfate attack. Applied Clay Science, 161, 70–75. https://doi.org/10.1016/j.clay.2018.04.014

Lee, A. R. (1974). Blastfurnace and steel slag: Production, properties and uses.

Lizarazo-Marriaga, J., Claisse, P., & Ganjian, E. (2011). Effect of steel slag and portland cement in the rate of hydration and strength of blast furnace slag pastes. Journal of Materials in Civil Engineering, 23(2), 153–160. https://doi.org/10.1061/(ASCE)MT.1943-5533.0000149

MacDonald, J. M., Brolly, C. V., Slaymark, C., Spruženiece, L., Wilson, C., & Hilderman, R. (2023a). The mechanisms and drivers of lithification in slag-dominated artificial ground. The Depositional Record, 9(4), 810-819. https://doi.org/10.1002/dep2.230

MacDonald, J. M., Khudhur, F. W. K., Carter, R., Plomer, B., Wilson, C., & Slaymark, C. (2023b). The mechanisms and microstructures of passive atmospheric CO2 mineralisation with slag at ambient conditions. Applied Geochemistry, 152, 105649. https://doi.org/10.1016/j.apgeochem.2023.105649

Mayes, W. M., Riley, A. L., Gomes, H. I., Brabham, P., Hamlyn, J., Pullin, H., & Renforth, P. (2018). Atmospheric CO2 Sequestration in Iron and Steel Slag: Consett, County Durham, United Kingdom. Environmental Science & Technology, 52(14), 7892–7900. https://doi.org/10.1021/acs.est.8b01883

McGrath, P. F., & Hooton, R. D. (1997). Influence of Binder Composition on Chloride Penetration Resistance of Concrete. Special Publication, 170, 331–348. https://doi.org/10.14359/6829

Mehta, P. K. (1983). Mechanism of sulfate attack on portland cement concrete—Another look. Cement and Concrete Research, 13(3), 401–406. https://doi.org/10.1016/0008-8846(83)90040-6

Miki, T., Futatsuka, T., Shitogiden, K., Nagasaka, T., & Hino, M. (2004). Dissolution Behavior of Environmentally Regulated Elements from Steelmaking Slag into Seawater. ISIJ International, 44(4), 762–769. https://doi.org/10.2355/isijinternational.44.762

Pan, S.-Y., Chang, E., & Chiang, P.-C. (2012). CO2 capture by accelerated carbonation of alkaline wastes: A review on its principles and applications. Aerosol and Air Quality Research, 12(5), 770–791.

Pane, I., & Hansen, W. (2005). Investigation of blended cement hydration by isothermal calorimetry and thermal analysis. Cement and Concrete Research, 35(6), 1155–1164. https://doi.org/10.1016/j.cemconres.2004.10.027

Piatak, N. M., & Ettler, V. (2021). Introduction: Metallurgical Slags – Environmental Liability or Valuable Resource? https://doi.org/10.1039/9781839164576-00001

Pranzini, E., & Williams, A. T. (2013). Coastal erosion and protection in Europe. Routledge London, UK.

Price, S. J., Ford, J. R., Cooper, A. H., & Neal, C. (2011). Humans as major geological and geomorphological agents in the Anthropocene: The significance of artificial ground in Great Britain. Philosophical Transactions of the Royal Society A: Mathematical, Physical and Engineering Sciences, 369(1938), 1056–1084. https://doi.org/10.1098/rsta.2010.0296

Pullin, H., Bray, A. W., Burke, I. T., Muir, D. D., Sapsford, D. J., Mayes, W. M., & Renforth, P. (2019). Atmospheric Carbon Capture Performance of Legacy Iron and Steel Waste. Environmental Science & Technology, 53(16), 9502–9511. https://doi.org/10.1021/acs.est.9b01265

Ragipani, R., Bhattacharya, S., & Suresh, A. K. (2019). Kinetics of steel slag dissolution: From experiments to modelling. Proceedings of the Royal Society A: Mathematical, Physical and Engineering Sciences, 475(2224), 20180830. https://doi.org/10.1098/rspa.2018.0830

Renforth, P. (2019). The negative emission potential of alkaline materials. Nature Communications, 10(1), 1401. https://doi.org/10.1038/s41467-019-09475-5

Renforth, P., Manning, D. A. C., & Lopez-Capel, E. (2009). Carbonate precipitation in artificial soils as a sink for atmospheric carbon dioxide. Applied Geochemistry, 24(9), 1757–1764. https://doi.org/10.1016/j.apgeochem.2009.05.005

Renforth, P., Washbourne, C.-L., Taylder, J., & Manning, D. A. C. (2011). Silicate Production and Availability for Mineral Carbonation. Environmental Science & Technology, 45(6), 2035–2041. https://doi.org/10.1021/es103241w

Riden, P., & Owen, J. G. (1995). British Blast Furnace Statistics, 1790-1980. Merton Priory.

Riley, A. L., MacDonald, J. M., Burke, I. T., Renforth, P., Jarvis, A. P., Hudson-Edwards, K. A., McKie, J., & Mayes, W. M. (2020). Legacy iron and steel wastes in the UK: Extent, resource potential, and management futures. Journal of Geochemical Exploration, 219, 106630. https://doi.org/10.1016/j.gexplo.2020.106630

Sanna, A., Uibu, M., Caramanna, G., Kuusik, R., & Maroto-Valer, M. (2014). A review of mineral carbonation technologies to sequester CO_2. Chemical Society Reviews, 43(23), 8049–8080. https://doi.org/10.1039/C4CS00035H

Scott, P. W., Critchley, S. R., & Wilkinson, F. C. F. (1986). The chemistry and mineralogy of some granulated and pelletized blastfurnace slags. Mineralogical Magazine, 50(355), 141–147. https://doi.org/10.1180/minmag.1986.050.355.19

Shi, C., Wang, D., & Behnood, A. (2012). Review of Thaumasite Sulfate Attack on Cement Mortar and Concrete. Journal of Materials in Civil Engineering, 24(12), 1450–1460. https://doi.org/10.1061/(ASCE)MT.1943-5533.0000530

Skelcher, G. (2014). Arnside & Silverdale Area of Outstanding Natural Beauty–Special Qualities Report. Arnside & Silverdale AONB.

Tian, B., & Cohen, M. D. (2000). Does gypsum formation during sulfate attack on concrete lead to expansion? Cement and Concrete Research, 30(1), 117–123. https://doi.org/10.1016/S0008-8846(99)00211-2

USGS. (2023). Iron and Steel Slag. Mineral Commodity Summaries.

Wilkinson, B. H. (2005). Humans as geologic agents: A deep-time perspective. Geology, 33(3), 161. https://doi.org/10.1130/G21108.1

Yi, H., Xu, G., Cheng, H., Wang, J., Wan, Y., & Chen, H. (2012). An Overview of Utilization of Steel Slag. Procedia Environmental Sciences, 16, 791–801. https://doi.org/10.1016/j.proenv.2012.10.108

Zhang, T., Yu, Q., Wei, J., Li, J., & Zhang, P. (2011). Preparation of high performance blended cements and reclamation of iron concentrate from basic oxygen furnace steel slag. Resources, Conservation and Recycling, 56(1), 48–55.